

RESEARCH ARTICLE

Open Access



Comparison of the LBM snowdrift model output with the observation results

Seika Tanji^{1*} , Masaru Inatsu^{2,3} and Yusuke Harada⁴

Abstract

In this work, snowdrift experiments which are equivalent to one drifting snow event are performed by the snowdrift model. The model consisted of the computational fluid dynamics part of the large-eddy simulation with the lattice Boltzmann method and the drifting snow part of the conventional advection algorithm for representative Lagrangian particles. The observed vertical wind profile of a 4 h drifting snow event in Teshikaga Town was used as the inflow boundary conditions in the model to compare the results of the snowdrift estimated by the model and the observed snowdrift distribution. Parallelization enabled us to simulate the snowdrift distribution in a realistic domain and on the time scale of a single drifting snow event. We demonstrated that the upgraded model could quantitatively reproduce the height and position of the observed snowdrift along the center of a three-dimensional fence.

Keywords Blowing snow, Drifting snow, Lattice Boltzmann method, Snowdrift, Snow fence

1 Introduction

Drifting snow is a phenomenon in which surface snow particles or snowfall particles are blown by a strong wind and often form snowdrifts in places where the wind speed is sufficiently low due to buildings and landforms. The numerical simulation of snowdrifts has overcome the limited observation opportunities of drifting snow events and the rough assumption of similarity in wind tunnel experiments. The most important issue in snowdrift simulation is resolving wind profiles at and above the surface because snow particles suspended in the air are advected by the background wind. Uematsu et al. (1991) and Liston et al. (1993) pioneered snowdrift simulation with wind profiles calculated by the Reynolds-averaged

Navier–Stokes equations model with turbulence parameterizations. A CFD (computational fluid dynamics) model for snowdrift simulation was developed into the LES (large-eddy simulation) with the finite differential method (Zwaafink et al. 2014; Okaze et al. 2018; Wang and Jia 2018).

A stumbling block for snowdrift simulation is demanding CFD calculations. CFD calculations on the order of centimeters are difficult for reproducing the observed snowdrift for model validation on a realistic spatial scale and event time scale. Tanji et al. (2021) developed a snowdrift model that contained the CFD part of the LES with the LBM (lattice Boltzmann method; McNamara and Zanetti 1988) and the drifting snow part of the conventional advection algorithm for representative Lagrangian particles. They showed that this model could be used for simulating snowdrifts based on the reasonable results from their idealized experiments. In addition, the LBM in this model had a simpler implementation and higher parallel computation efficiency than the conventional CFD algorithms (Chen and Doolen 1998; Han et al. 2019). Hence, parallelizing the model should enable us to perform snowdrift experiments with a full three-dimensional CFD computation for a sufficiently large domain

*Correspondence:

Seika Tanji
seika@storm.dpri.kyoto-u.ac.jp

¹ Disaster Prevention Research Institute, Kyoto University, Gokasho, Uji, Kyoto 6110011, Japan

² Faculty of Science, Hokkaido University, N10W8, Sapporo 0600810, Japan

³ Center for Natural Hazards Research, Hokkaido University, N9W9, Sapporo 0608589, Japan

⁴ Civil Engineering Research Institute for Cold Region, 1-34 1-13 Hiragishi, Tohohira-Ku, Sapporo 0628602, Japan

and long-time integration, which has not been achieved yet.

Here, this paper aims to enable to conduct a long-run numerical simulation which is equivalent to one drifting snow event and reproduce an observed snowdrift distribution quantitatively by parallelizing the model developed by Tanji et al. (2021). The snowdrift part of the model was also upgraded to allow quantitative treatment of drifting snow particles. We added resuspension and rebound processes that seemed non-negligible, but excluded splash (Sugiura and Maeno 2000) and sublimation that likely contributed little to snowdrift formation in the calculation domain and time scale in this study (Okaze et al. 2018; Palm et al. 2017; Zwaafink et al. 2013). The experiments in this study were limited to the time scale for snow accumulation upstream of obstacles, here a solid fence, so that we ruled out the interaction between fluid dynamics and snow surface change. Because there was no turbulent wind observation in the full domain, we imposed the laminar flow fit to the single-point anemometer observations as the upstream boundary after we checked that the turbulent inflow did not substantially affect the snowdrift results in advance. The remaining part of this paper is organized as follows. We introduce the observation data in Sect. 2 and the model upgraded from Tanji et al. (2021) in Sect. 3; we describe the experiment settings in Sect. 4; we show the

simulation results of the snowdrift distribution and compare it with the observations in Sects. 5; and we conclude the paper in Sect. 6.

2 Observation data

We used observation data acquired in Teshikaga, Hokkaido, Japan (43.502° N and 144.467° E; Fig. 1; Okaze et al. 2019). This site was a flat field with no obstacle over 500 m on the windward side of the observation point. On the site, wind speed and direction were observed every 10 min with three-dimensional ultrasonic anemometers at four levels of the observation tower, at heights of about 1, 1.5, 3, and 7 m above the surface. The number of drifting snow particles passing the specific area was also measured at the same levels by SPCs (snow particle counters) with every second output. The solid, non-porous fence was 6 m long, 4 mm thick, and 1 m high and was set in the field (Fig. 2a). The sensors of ultrasonic anemometers and SPCs and the fence are located on almost the same line perpendicularly to the dominant wind direction.

On February 18, 2019, strong wind and drifting snow were recorded in the morning, and a snowdrift was formed around the fence. The day before the drifting snow event, there had been snowfall with light wind, and the field was uniformly covered with snow about 2 cm depth. However, no snowfall was recorded, while the drifting snow was developing on February 18 according

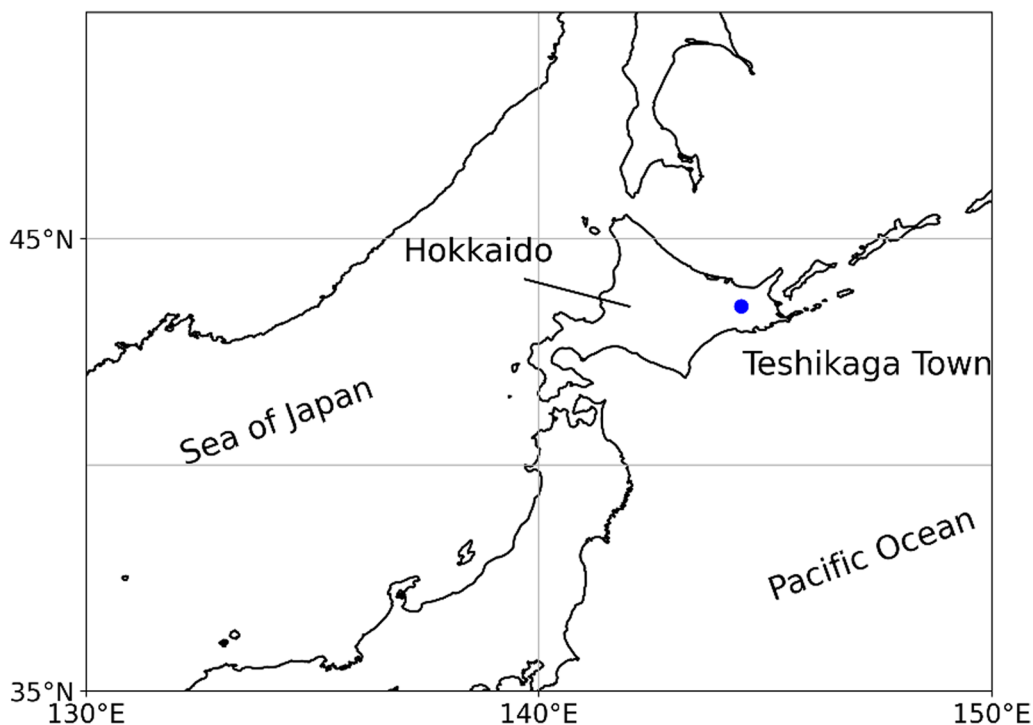


Fig. 1 Map of northern Japan and surrounding area. The blue circle denotes the observation site in Teshikaga Town



Fig. 2 **a** Photograph showing the observation tower loaded with anemometers and snow particle counters and the fence at the observation site. **b** Photograph showing the measurement of snowdrift height in the cross section along the center of the fence. Vectors show the main wind directions at the site. These photographs were taken on another day, not related to the event that we examined

to the observations from a heated rain gauge at an AMEDAS (Automated Meteorological Data Acquisition System) point near the site (43.51° N and 144.45° E). On the day following the drifting snow event, the snowdrift height was measured in the cross section normal to the fence at its center (Fig. 2b).

3 Method

3.1 CFD module

The CFD module was the same as in Tanji et al. (2021), but the program was fully parallelized. The module was an LBM LES model with the D3Q19 configuration, which calculated the friction velocities of 3-dimensional 19 directions. The single relaxation time was imposed as a collision operator. The subgrid scale parameterization was applied to estimate the eddy kinematic viscosity (Smagorinsky 1963; Feng et al. 2007; Onodera et al. 2013; Wang et al. 2014; Suga et al. 2015). Different from Tanji et al. (2021), the non-dimensional viscosity of the air which was changed to 2.0×10^{-6} to simulate the flow with a higher Reynolds number.

We set the model domain to a three-dimensional channel, which was almost the same with the three-dimensional fence experiment in Tanji et al. (2021). We defined wind direction, x axis, as from the western to eastern boundaries. The model coordinate is set as x axis for the wind direction, y axis for the fence direction normal to the wind and z axis for the vertical direction. The boundary conditions were the same as Tanji et al. (2021), but the initial and the inflow conditions on the western boundary were replaced with observation data (Sect. 4.1). The east, bottom, and top boundaries were free flow, no-slip, and free-slip conditions, respectively. The north and south boundaries conditions were imposed on cyclic.

3.2 Snow particle module

The snow particle module consisted of moving, deposition, resuspension, and rebound; the latter two were added to the model developed in Tanji et al. (2021). The resuspension is the process that snow particles on the surface are peeled off by the strong wind, and the rebound is the process that snow particles bound on the surface mechanically.

The moving process described the blown snow particles in the air by the wind calculated by the CFD module with referred to Nishimura and Hunt (2000). The method assumed that the drifting snow particles are spherical and calculated the particles' speed related to the wind flow and drag coefficient. We set the particle diameter to $135 \mu\text{m}$ and density of particles to 910 kg m^{-3} (Nishimura and Hunt 2000). The given diameter was close to the average diameter of $135 \mu\text{m}$ observed at heights of 1 and 1.5 m at the site because snow particles following at lower levels contribute to snowdrift formation (Tanji et al. 2021).

The resuspension process was activated when the wind speed near the surface was strong enough to peel off accumulated snow particles on the surface. The threshold value of the resuspension is decided by the friction velocity following Clifton et al. (2006) as

$$u_{*t} = 0.2 \sqrt{\frac{\rho_p - \rho_a}{\rho_a} g d}, \quad (1)$$

where g is the gravity (9.8 m s^{-2}), ρ_a is the densities of air (1.34 kg m^{-3}), d is the particle diameter, and ρ_p is the density of snow particles. The threshold value was about 0.189 m s^{-1} in the condition of this study. The friction velocity on each grid was estimated by Werner and Wenglem (1991) (see Tanji et al. 2021). A snow particle was launched from a grid where the friction velocity exceeded the threshold gd value. The initial velocity of

the resuspended particle was equal to the wind speed at one grid above the resuspended point. A single particle represented snow mass corresponding to the volume of snow on the grid (Sect. 4.1). A launched particle was suspended in the air, and the volume was released when the particle accumulated on the surface.

A snow particle that reached the surface proceeded to the rebound or the deposition process. The process after a collision was determined by the kinetic energy of the snow particle. If the particle velocity after the collision with the surface was enough for the particle to bounce by one grid height in the CFD calculation, 5 cm, the particle rebounded. Otherwise, the particle proceeded to the deposition process and stayed unless the friction velocity there was strong enough to activate the resuspension process. Elevation angle θ_r , azimuth angle φ_r , and restitution coefficient e_r were estimated when particles collided with the surface (Fig. 3). Although Okaze et al. (2018) suggested that these parameters follow the normal distributions, we gave the fixed values as a function of incident angle θ_{in} as elevation angle $\theta_r = 20^\circ + 0.19\theta_{in}$, azimuth angle $\varphi_r = 0$, and restitution coefficient $e_r = 0.87 - 0.62\sin\theta_{in}$, which were the averaged value in Okaze et al. (2018). We also assumed that a particle would consecutively rebound 50 times at most because a few particles continuously rebounded in the same grid.

4 Experiments

4.1 Inflow condition

The imposed wind profile as the initial condition and the western boundary condition in the CFD module was the laminar logarithmic profile with the roughness length for a flat snow surface $z_0 = 0.1$ (mm) (Nishio and Ishida 1973)

$$u_0(z) = \frac{u_*}{\kappa} \ln\left(\frac{z}{z_0}\right), \quad (2)$$

where von Karman's constant $\kappa = 0.4$. The friction velocity was determined by observed wind data using the

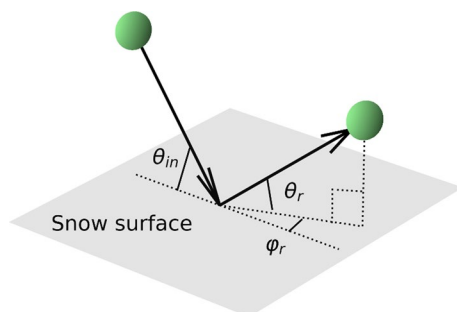


Fig. 3 Schematic of incident angle θ_{in} , elevation angle θ_r , and azimuth angle φ_r in the rebound process. Green spheres show snow particles

least squares method by the following procedure. First, we chose the period of the drifting snow event from the observed wind data and the amount of drifting snow data and averaged the wind data at each height over the period. Second, we decided the friction velocity in Eq. (2) with the minimum root mean square error between the averaged observation data and the logarithmic profile. Finally, we obtained the logarithmic profile, which was close to the observation results. In this paper, we did not apply artificial inflow turbulence as the inflow condition because the inflow turbulence did not substantially affect the results for snowdrifts on the windward side of the fence, as shown in Additional file 1.

The amount of inflow snow particles from the western boundary was also estimated by the logarithmic profile decided above. We did not directly use SPCs data as the amount of inflow snow particles. This was because the vertical number of SPCs was insufficient at lower level where inflow snow particles largely contributed to the snowdrift formation (Tanji et al. 2021). Instead, following Tanji et al. (2021), snow particles were initially arranged in a grid of 5 cm in horizontal direction by 2.5 cm in vertical direction on the inflow plane. A single particle in this model represented snow mass corresponding to snow volume flux v_f ($\text{m}^3\text{m}^{-2}\text{s}^{-1}$) depending on the height with referred to Shiotani (1953) and Matsuzawa and Takeuchi (2002) as

$$v_f(z) = \alpha \frac{\min\left(30, 30\left(\frac{z}{0.15}\right)^{-\frac{0.30}{\kappa u_*}}\right) u_0(z)}{\rho_p} / \beta. \quad (3)$$

It was noted that α and β were the constants to ensure consistency with the period of the drifting snow event and to relate to snowdrift density, respectively. We set β to 0.5 for compacting snow particles, which was consistent with the condition in the site because continuous snowfall was recorded at the nearest AMeDAS site on the day before the drifting snow event. It had enough time to form the compacting snow layer. The friction velocity u_* was estimated by the method in the prior paragraph. The reference height and snow concentration in Eq. (3) referred to Matsuzawa and Takeuchi (2002).

4.2 Simulation set-up

The simulation domain covered 18 m width by 15 m depth by 5 m height on a grid spacing of 0.05 m (Fig. 4). The solid fence in the simulation was set at the center of the y -axis and located at $x = 0$, which was 5 m from the western boundary. The fence was 6 m length, 0.1 m thickness, and 1 m height. The integration time of the CFD calculation was 3600 s after a spin-up of 30 s because it took about 10 s to stabilize the calculation

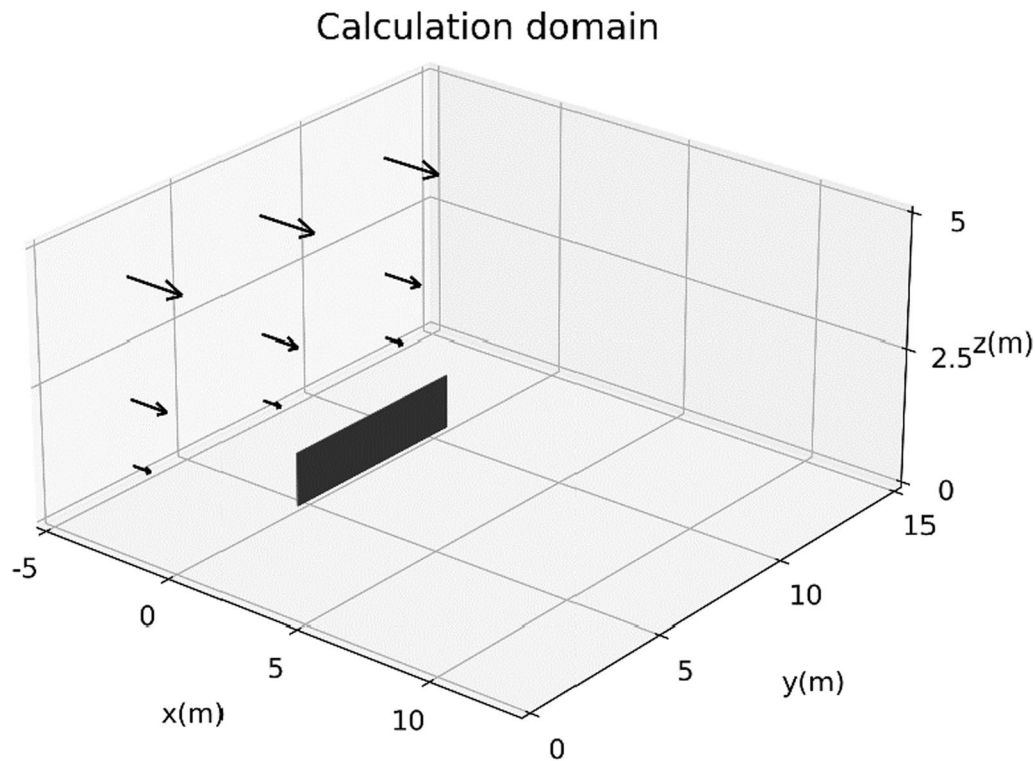


Fig. 4 Schematic of the calculation domain and the initial wind vectors in the experiments. The black panel at $x = 0$ is the fence

(not shown), the time step was 0.5 ms, and the result output was every 1 s.

We calculated trajectories of a finite number of snow particles in the snow particle module with a time interval of 1 ms until all particles were deposited. The snow particle calculations were conducted with several initial times for the wind, and the snowdrift result was the sum of the members' results (Fig. 5). The initial wind profile was given to the snow particle module every second (total of 3600 members), and the wind profile was renewed every second in the calculation. The wind profile data at 3600 s were constantly imposed when the calculation extended beyond 3600 s. When a snow particle fell on the surface, the snow volume defined in Eq. (3) was released and made snowdrift on the grid. It was noted that snow particles did not collapse and were not eliminated by melting or sublimation processes in this simulation. This model excluded the splash that snow particles pop up from the snow surface due to impact of other snow particles collided the surface, because we only calculated limited representative particles mentioned in Sect. 4.1. According to Okaze et al. (2018), it showed the rebound particles was much greater than splash particles and the rebound process was more dominant than the splash around the surface.

5 Results

5.1 Inflow condition

Figure 6 shows the observed time series of the wind speed and snow volume flux on February 18, 2019. We calculated the snow volume flux by the SPC outputs which measured numbers of snow particles passing the sensor phase and their diameter. The wind speed and snow volume flux were large between 0830 and 1300 JST (JST = UTC + 9), with a peak at about 1010 and 1040 JST, respectively. The highest wind speed was over 11 ms^{-1} at a height of 7 m and the largest snow volume flux was about $8 \times 10^{-4} \text{ m}^3 \text{ m}^{-2} 10 \text{ min}^{-1}$ at a height of 1 m in the period. The wind speed dropped to under 6 ms^{-1} after 1500 JST.

Figure 7 shows the vertical profiles of the observed wind speed averaged over former 1 h and the wind speed estimated with the least squares method. The estimated wind speed at each time almost corresponded to the observed values and increased during the drifting snow event from 1000 to 1200 JST (Fig. 7b–d), although there was a slight difference between the estimated and observed wind speed at a height of 3 m. The snow volume flux was calculated by Eq. (3) with these logarithmic wind profiles. The estimated amount of the snow volume flux overestimated the observations below a height

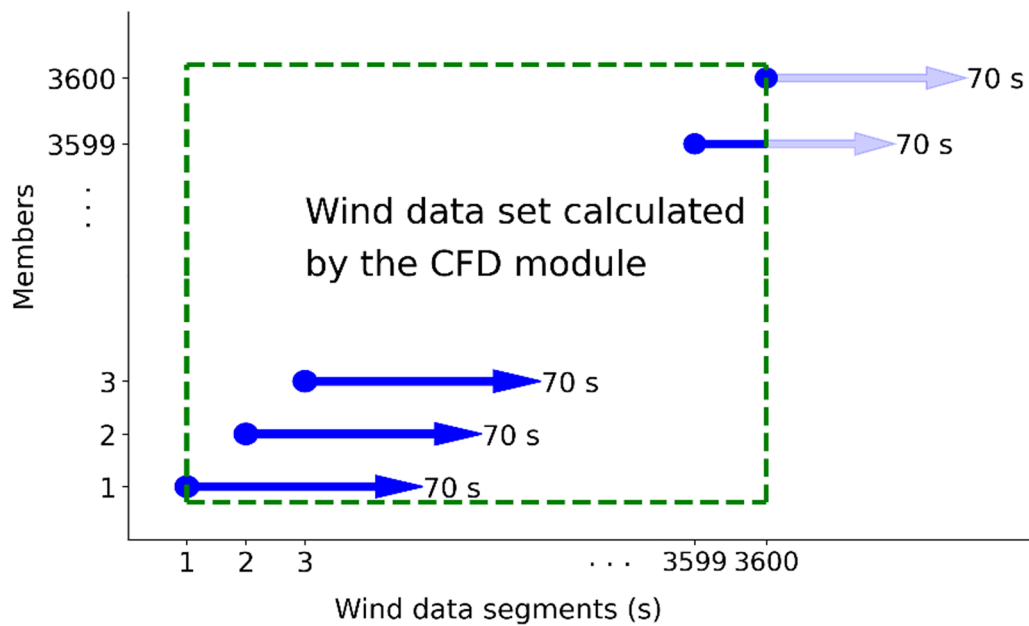


Fig. 5 Schematic of the wind data set calculated in the computational fluid dynamics (CFD) module and its treatment in the snow particle module. Blue vectors show that we calculate the snow particles' movements for a maximum of 70 s

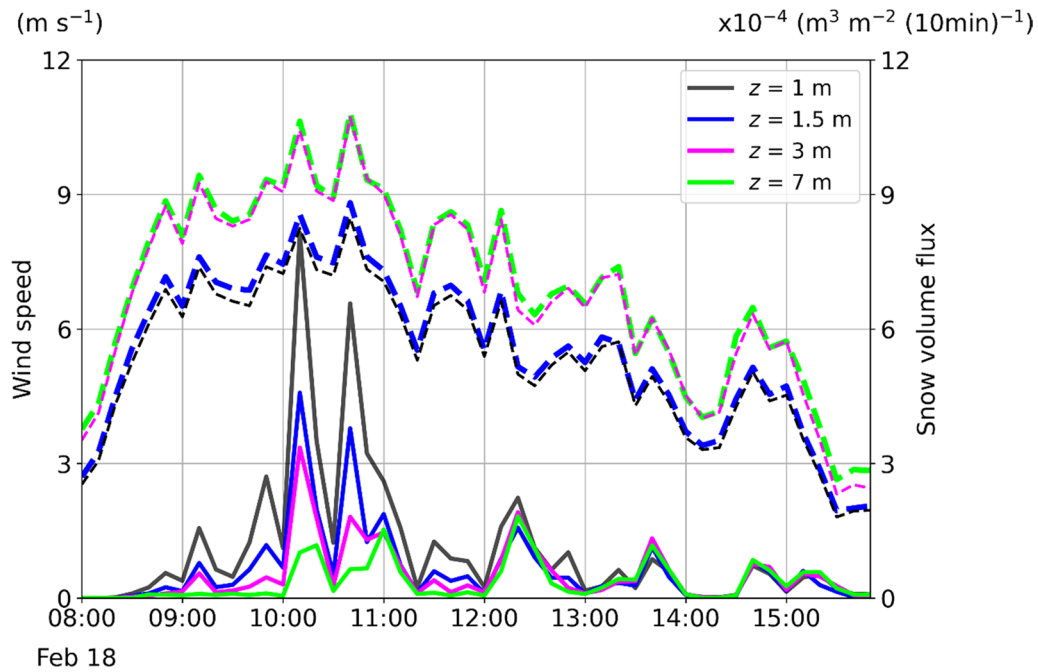


Fig. 6 Time series of the observed wind (dotted lines) and snow volume flux (solid lines) at heights of (black) 1 m, (blue) 1.5 m, (pink) 3 m, and (green) 7 m from 08:00 to 16:00 JST on 18 February 2019

of 4 m, especially during the drifting snow event (Fig. 8). However, the estimated vertical profiles of the snow volume flux clearly indicated the observed feature of larger snow volume flux at lower levels during the drifting snow

event. Therefore, we decided that the 4 h drifting snow event occurred from 900 to 1300 JST, and α of Eq. (3) was set to 4 because the observed snow volume flux increased in this period (Fig. 8b–e).

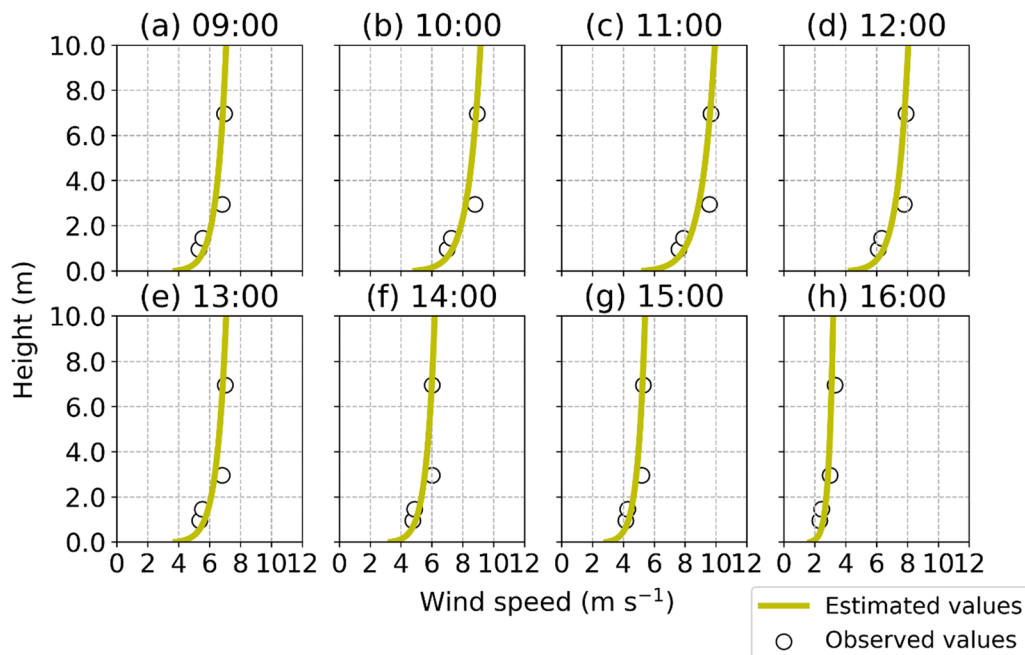


Fig. 7 Averaged vertical wind profiles every hour from (a) 09:00 to (h) 16:00 JST. Yellow lines show the log profiles estimated with the least squares method, and open circles show the observed values

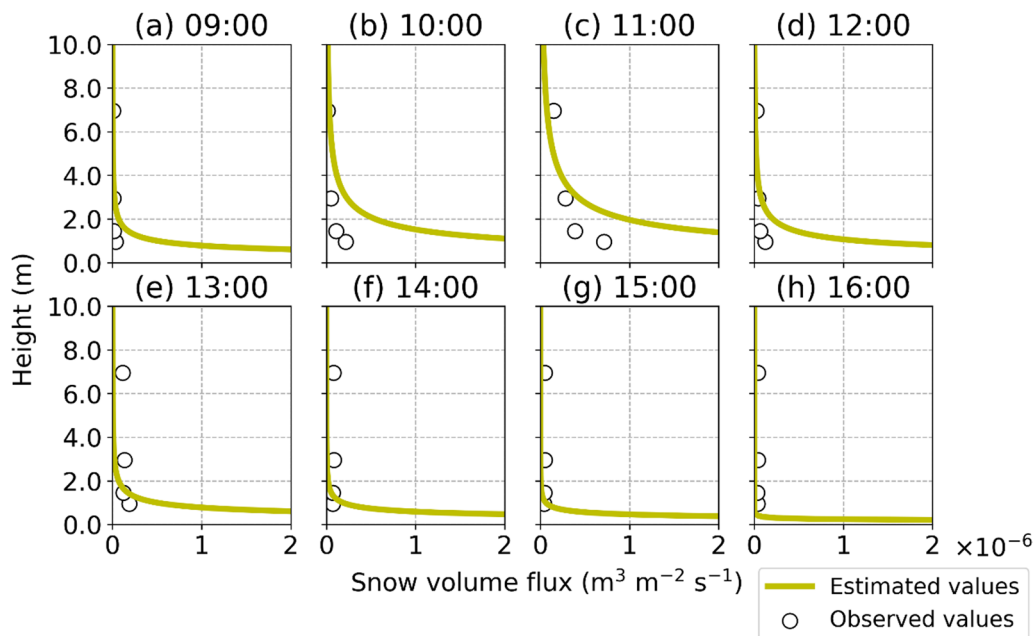


Fig. 8 Averaged snow volume flux profiles every hour from (a) 09:00 to (h) 16:00 JST. Yellow lines show the values estimated using Eq. (2) and the wind profiles in Fig. 7. Open circles show the observed values

Figure 9 shows the averaged vertical profiles of the wind speed and snow volume flux over the 4 h drifting snow event in the observation. The friction velocity was estimated as 0.297ms^{-1} with the least squares method.

The estimated wind profile (Fig. 9a) almost corresponded to the observed values. The snow volume flux estimated by the friction velocity was still larger than the observed data at lower heights. The estimated snow volume flux

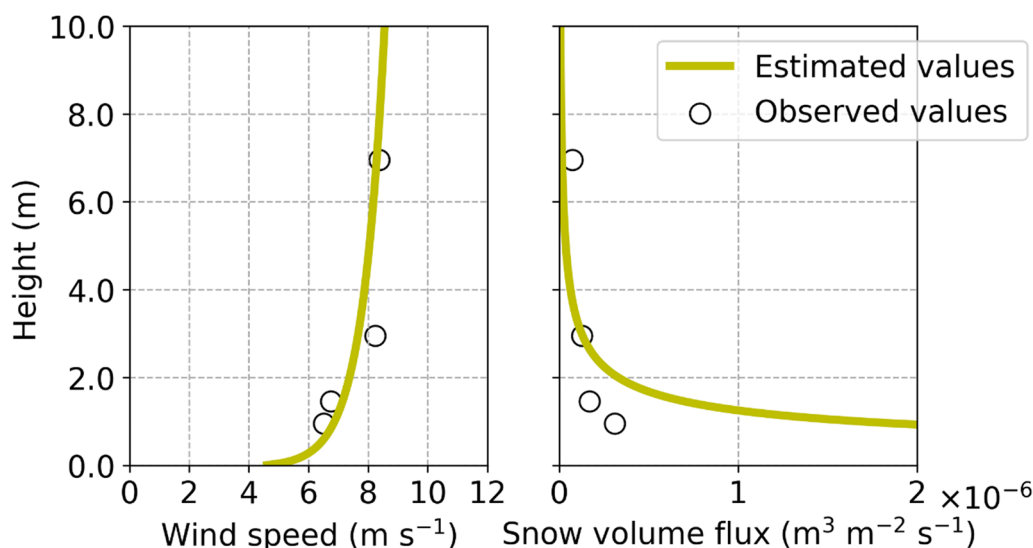


Fig. 9 Vertical profiles used in the model of the wind speed and the snow volume flux averaged over the drifting snow period. Yellow lines show the estimated profiles, and circles show the observed values

$1.9 \times 10^{-6} \text{ m}^3 \text{ m}^{-2} \text{ s}^{-1}$ was equivalent to the volume of $1.5 \times 10^6 \text{ m}^{-2} \text{ s}^{-1}$ snow particles with $135 \mu\text{m}$ diameter at a height of 1 m. However, we considered that the estimated profile was in the range of uncertainty in the observed data because the maximum of the observed snow volume flux was one or two orders larger per second than the averaged observation data, especially at a height of 1 m. The estimated wind profiles were given as the western boundary condition in the CFD module, and the amount of the inflow snow was given in the snow particle module.

5.2 Model results

Figure 10 shows a snapshot of the wind profiles at the end of the calculation in the CFD module. The vertical wind profile had three obvious features, which were a stagnation area formed around the front of the fence, stronger wind speed at the top of the fence, and reverse flow developed behind the fence from $x = 0$ – 5 m (Fig. 10a). The reverse flow behind the fence was clearer on the horizontal wind profile (Fig. 10b). The wind flow horizontally forked around the fence, and there was a dipole pattern from $x = 0$ – 4 m along $y = 5$ and 10 m. The qualitatively features of the vertical and horizontal wind profiles were consistent with previous simulation studies (Han et al. 2021; Tanji et al. 2021).

Figure 11a shows the model result of the snowdrift distribution around the fence. The higher snowdrift was closer to the fence on the windward side, but the height of the snowdrift just in front of the fence was low. The snowdrift height estimated by the model agreed with the observed profile in the cross section along the center of

the fence (Fig. 11b), with a peak around $x = -1.5$ m and a peak height of about 0.41 m. Many previous simulation studies (Uematsu et al. 1991; Alhajraf 2004; Tanji et al. 2021) and the previous observation (Tabler 1994) also showed this outline form of the snowdrift. This snowdrift formation was caused by the slower wind speed near the fence (Fig. 10a). The results for the snowdrift with half the amount of inflow particles are shown in Fig. 11b to demonstrate the growth process of the snowdrift. The result showed that the snowdrift around the inflow boundary mainly grew. The snowdrift nearer the fence was formed later by the snow particles that reached there by the repeat resuspension and rebound processes from the mature snowdrift surface. Snowdrifts with heights of about 0.45 m were displayed from $x = -0.1$ – 0 m only in the model, contrary to the observations with a small snowdrift just behind the fence around $x = 0.5$ m (Fig. 11b). The difference could be because of a small gap between the panel and the snow surface at the observation site. Some snow particles were blown to the leeward side of the fence from the gap and accumulated just behind the fence. This gap could cause the differences in the snowdrift height between the simulation and observations around $x = 0$ m.

The snowdrift distribution on the leeward side of the fence had an arc formation in the no-fence zone, but the snowdrift was not formed just behind the fence. These features were consistent with previous simulation studies (Beyers et al. 2004; Okaze et al. 2013; Tanji et al. 2021). The arc formations were made by snow particles following the split flow from the sides of the fence (Fig. 10b). Few snow particles in the flow reached just behind the

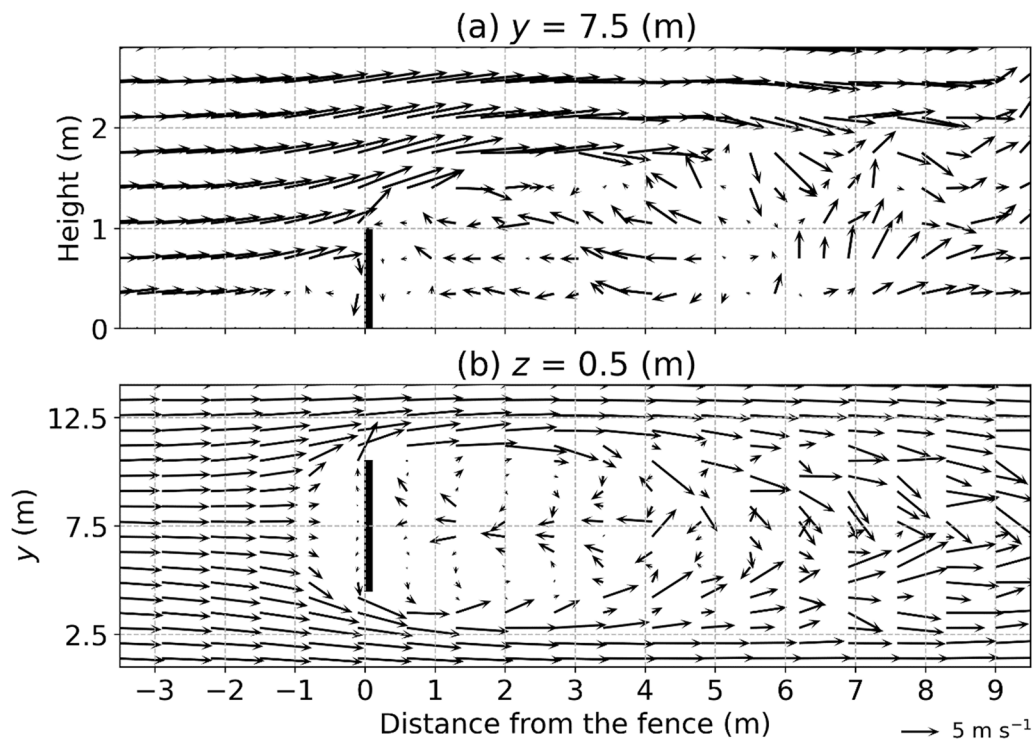


Fig. 10 Snapshots of the wind vectors around the fence at the last segment in the cross section along **a** $y = 7.5$ m and **b** $z = 0.5$ m. The solid lines at $x = 0$ show the fences

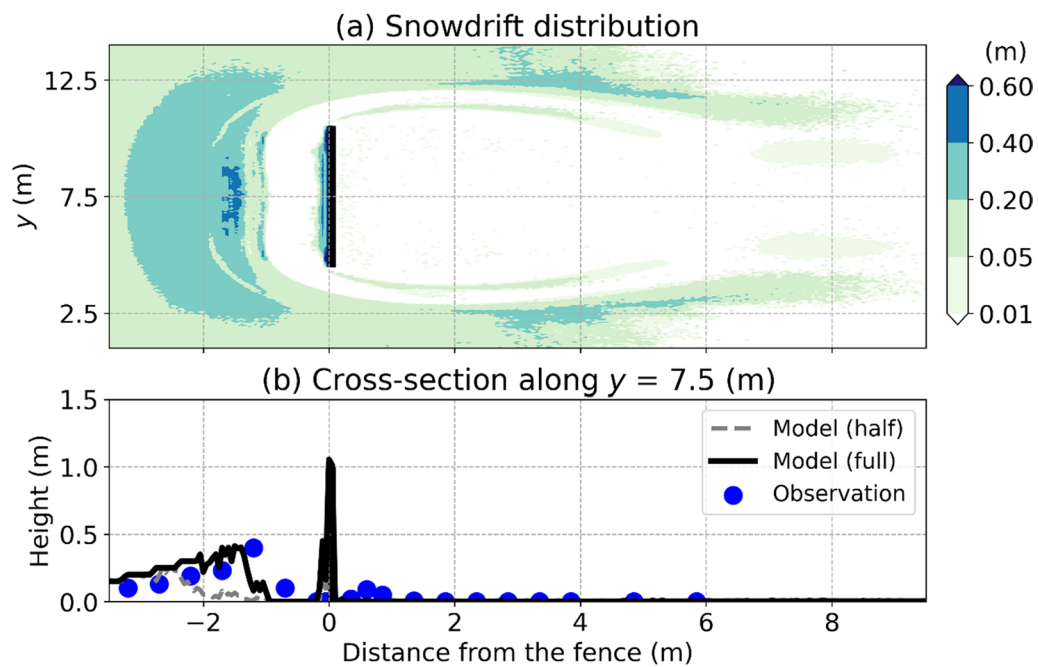


Fig. 11 **a** Snowdrift height distribution around the fence. **b** Snowdrift height in the cross section along $y = 7.5$ m at (solid) 1 h and (dotted) 0.5 h lead times. The blue circles show the observed heights

fence, and almost no snowdrift was formed along the center of the fence on the leeward side in both the simulation and observations (Fig. 11b). The peak of the snowdrift on the leeward side was $y = 12.5$ and 2.5 m from $x = 3$ to 4 m.

6 Conclusions and discussion

In this work, we upgraded the LBM-based snowdrift model developed by Tanji et al. (2021) with parallelization and a quantitative treatment for snow particles, which enabled us to perform high-speed, long-run, and practical simulation of the snowdrift. We conducted full three-dimensional CFD and snow particle computation that reproduced snowdrifts along the center of the fence observed after one case of the drifting snow event in the flat snowy environment at Teshikaga, Japan. In the experiment, we used the observed vertical wind profile at the Teshikaga site as the inflow boundary conditions in the model. The numerical simulation was conducted in a finite channel containing a finite solid fence, mimicking the observation site. The simulated result of the snowdrift height corresponded to the observed snowdrift height along the center of the fence. We demonstrated that the upgraded model reproduced the observed snowdrift distribution along the center of the snow fence quantitatively (Additional file 1).

We did not directly use the observed amount of drifting snow particles as the boundary condition due to the insufficient vertical resolution above the snow surface. Instead, we used the estimated value of the observed wind data. Tanji et al. (2021) showed that the inflow snow particles from under 1 m height above the surface are important in forming the snowdrift around the 1 m-high fence. However, measuring snow volume flux just above the surface is difficult because the observation instruments can be buried in the snowdrift during the events. Even the trench method, in which the number of snow particles is measured in trenches on the surface (Nishimura 2009), is not practical currently due to its high costs. Hence, the estimation of the inflow snow particles in this paper is practical if the assumption of the logarithmic wind profile [Eq. (2)] is valid.

The model validation in this study was done by comparison with the one-dimensional observation data for snow accumulation along the center of the fence. This gauge observation of the cross section at the fence center did not show whether the fork structure on the leeward side of the fence was well simulated in the model. Photogrammetry and LiDAR (light detection and ranging) have been used to measure the horizontal distribution of snowdrift heights. Photogrammetry mainly uses photographs taken by UAVs (unmanned aerial vehicles). Niiya et al. (2021) took aerial images from a UAV before and

after a drifting snow event and made a digital surface model of a snowdrift around a snow fence. The estimated snowdrift height was consistent with the cross-sectional observation. Although photogrammetry is a useful tool for observing snowdrifts, UAVs cannot fly under strong wind conditions and images cannot be taken at night. LiDAR can mitigate these disadvantages of photogrammetry because the method measures reflected near-infrared radiation or ultraviolet radiation. LiDAR can also observe the snowdrift growing during a drifting snow event. Okaze et al. (2022) showed that the snowdrift distribution observed by LiDAR corresponded to that observed by photogrammetry. Ohara et al. (2022) compared a snowdrift model simulation with these observations. We will validate our model with these methods in future work.

The numerical simulation model in this study ignored the splash process and the sublimation process of snow particles, which were often implemented in the model of drifting snow in the previous studies. The splash process was considered not to contribute to the snowdrift distribution in this situation because of more rarely development than the rebound process, as mentioned in Sect. 4. However, previous studies suggested that the splash process had an important role to the development of the drifting snow (Niiya and Nishimura. 2022; Zwaafink et al. 2014). Therefore, the splash process is required when we simulate the beginning of the drifting snow event explicitly. The sublimation process also does not have the impact on the snowdrift distribution because the amount of snow is lost by the sublimation in the upper area of the drifting snow development. The upper height had little snow volume flux during the drifting snow event (Figs. 8, 9). In addition, Tanji et al. (2021) demonstrated that few snow particles inflowing from over 1.5 m height fell on around the fence and most of them were blown to out of the calculation domain. The sublimation process can be important in the discussion about the hydrological cycle and surface water mass balance during the entire winter season in the cryosphere (Zwaafink et al. 2013; Palm et al. 2017).

The present model in this study remained some room for improvement, but the model had the potential to be applied to resolving many problems caused by snowdrifts around roads. Snow fences have been installed on the side of the roads to protect the roads from snowdrifts on the leeward. However, no one knows which snow fence structures are optimal for preventing snowdrifts developing on roads. The LBM snowdrift model is suitable for researching structures in many experiments because the model has high parallel computation efficiency. Snowdrifts that form around the lateral gap between snow fences are also a serious problem for

road administration because gaps are required at intersections. Snowdrifts around the various road structures can be estimated with this model. This model also can be used to estimate visibility due to drifting snow on roads, which is the main cause of traffic disruption in snowy areas. Visibility due to drifting snow is related to the amount of snowdrift flux (Budd et al. 1966; Takeuchi and Fukuzawa 1976; Matsuzawa and Takeuchi 2002). The amount of drift snow transport can be calculated explicitly in this model by tracing drifting snow particles.

In mountainous areas, the redistribution of snow particles by drifting snow plays an important role in snow cover distribution and contributes to the avalanche potential, but previous studies did not calculate the redistribution explicitly (Bartelt and Lehning 2002; Brun et al. 1992). The boundary conditions and snowdrift distribution in mountainous areas are more complicated than those around a snow fence, although the LBM can still calculate the turbulent flow because it is suitable for complicated boundary conditions. Tracing drifting snow particles is also helpful for estimating the avalanche potential because the potential is strongly associated with the condition of the snowpack layers. The snowpack layer consisting of drifting snow particles has different features from that consisting of snowfall particles because the shape of the particles is different. Therefore, the model in this paper has the potential to resolve problems caused by drifting snow in mountainous areas.

Abbreviations

AMeDAS	Automated Meteorological Data Acquisition System
CFD	Computational fluid dynamics
LBM	Lattice Boltzmann method
LES	Large-eddy simulation
LiDAR	Light detection and ranging
SPC	Snow particle counter
UAV	Unmanned aerial vehicle

Supplementary Information

The online version contains supplementary material available at <https://doi.org/10.1186/s40645-023-00599-3>.

Additional file 1. Supplementary Material.

Acknowledgements

We thank Dr. Yousuke Sato for teaching basic parallelization. We are very grateful to Dr. Satoshi Omiya for supporting us in the observations. We also thank Dr. Tsubasa Okaze, Dr. Hirofumi Niiya, Dr. Masaki Nemoto, and Prof. Kouichi Nishimura for providing insightful comments in the early stage of this study.

Author contributions

ST, the main author, contributed to this paper, conceived and designed the study, developed the source code of the snowdrift model, analyzed the model results, and wrote the manuscript. MI, the second author, helped in the development of the snowdrift model, interpretation of the results, and writing the manuscript. YH contributed to observation work and acquired and analyzed the observed data in this study.

Funding

ST was supported by JST SPRING, Grant Number JPMJSP2119. MI is supported by JSPS KAKENHI Grant No. 19H00963, by the Environment Research and Technology Development Fund JPMEERF20232003 of the Environmental Restoration and Conservation Agency provided by Ministry of the Environment of Japan, and by Research Field of Hokkaido Weather Forecast and Technology Development (endowed by Hokkaido Weather Technology Center Co., Ltd.). MI and YH were supported by grant number JPMXD0722680734 from the Ministry of Education, Sports, Culture, Science and Technology (MEXT). This work was partly performed by using the supercomputer system at the Information Initiative Center, Hokkaido University, Sapporo, Japan.

Availability of data and materials

The datasets used during the current study are available from the corresponding author on reasonable request.

Declarations

Competing interests

The authors declare that they have no competing interests.

Received: 2 June 2023 Accepted: 9 November 2023

Published online: 29 November 2023

References

- Alhajraf S (2004) Computational fluid dynamic modeling of drifting particles at porous fences. *Env Modelling Softw* 19:163–170. [https://doi.org/10.1016/S1364-8152\(03\)00118-X](https://doi.org/10.1016/S1364-8152(03)00118-X)
- Bartelt P, Lehning M (2002) A physical SNOWPACK model for the Swiss avalanche warning. Part I. numerical model. *Cold Reg Sci Tech* 35(3):123–145. [https://doi.org/10.1016/S0165-232X\(02\)00074-5](https://doi.org/10.1016/S0165-232X(02)00074-5)
- Beyers JHM, Sundsbo PA, Harms TM (2004) Numerical simulation of three-dimensional, transient snow drifting around a cube. *J Wind Eng Ind Aerodyn* 92:725–747. <https://doi.org/10.1016/j.jweia.2004.03.011>
- Brun E, David P, Sudul M, Brunot G (1992) A numerical-model to simulate snow-cover stratigraphy for operational avalanche forecasting. *J Glaciol* 38(128):13–22. <https://doi.org/10.3198/1992JoG38-128-13-22>
- Budd WF, Dingle R, Radok U (1966) The byrd snow drift project: outline and basic results. *Studies in antarctic meteorology. Antarct Res Ser* 9:71–134. <https://doi.org/10.1029/AR009p0071>
- Chen S, Doolen GD (1998) Lattice Boltzmann method for fluid flows. *Annu Rev Fluid Mech* 30:329–364. <https://doi.org/10.1146/annurev.fluid.30.1.329>
- Clifton A, Rüedi JD, Lehning M (2006) Snow saltation threshold measurements in a drifting snow wind tunnel. *J Glaciol* 39:585–596. <https://doi.org/10.3189/172756506781828430>
- Feng YT, Han K, Owen DRJ (2007) Coupled lattice Boltzmann method and discrete element modelling of particle transport in turbulent fluid flows: Computational issues. *Int J Numer Meth Engng* 72:1111–1134. <https://doi.org/10.1002/nme.2114>
- Han M, Ooka R, Kikumoto H (2019) Lattice Boltzmann method-based large-eddy simulation of indoor isothermal airflow. *Int J Heat Mass Transf* 130:700–709. <https://doi.org/10.1016/j.jheatmasstransfer.2018.10.137>
- Han M, Ooka R, Kikumoto H (2021) Effects of wall function model in lattice Boltzmann method-based large-eddy simulation on built environment flows. *Build Environ* 195:107764. <https://doi.org/10.1016/j.buildenv.2021.107764>
- Hecht M, Harting J (2010) Implementation of on-site velocity boundary conditions for D3Q19 lattice Boltzmann simulations. *J Stat Mech* P01018. <https://doi.org/10.1088/1742-5468/2010/01/P01018>
- Inagaki A, Kanda M, Ahmad HN, Yagi A, Onodera N, Aoki T (2017) A numerical study of turbulence statistics and the structure of a spatially-developing boundary layer over a realistic urban geometry. *Bound-Layer Meteorol* 164:1651–2181. <https://doi.org/10.1007/s10546-017-0249-y>
- Liston GE, Brown RL, Dent JD (1993) A two-dimensional computational model of turbulent atmospheric surface flows with drifting snow. *Ann Glaciol* 18:281–286. <https://doi.org/10.3189/S0260305500011654>

- Matsuzawa M, Takeuchi M (2002) A study of methods to estimate visibility based on weather conditions. *Seppyo* 64:77–85. <https://doi.org/10.5331/SEPPYO.64.77> (in Japanese)
- McNamara GR, Zanetti G (1988) Use of the Boltzmann equation to simulate lattice-gas automata. *Phys Rev Lett* 61:2332–2335. <https://doi.org/10.1103/PhysRevLett.61.2332>
- Niia H, Nishimura K (2022) Hysteresis and surface shear stresses during snow-particle aeolian transportation. *Bound-Layer Meteorol* 183:447–467. <https://doi.org/10.1007/s10546-022-00688-8>
- Niia H, Omiya S, Sunako S, Nishimura K, Okaze T (2021) Snowdrift observation around fence by UAV-SfM photogrammetry. *JSSI JSSE Joint Conference 2021 in Online* (in Japanese)
- Nishimura K (2009) Measurement of Blowing Snow. *Nagare* 28:455–460 (in Japanese)
- Nishimura K, Hunt JCR (2000) Saltation and incipient suspension above a flat particle bed below a turbulent boundary layer. *J Fluid Mech* 417:77–102. <https://doi.org/10.1017/S002211200001014>
- Nishio F, Ishida T (1973) Rate of Turbulent Energy Dissipation During Snow Drifting. *Low Temp. Sci. Series A Phys Sci* 31:69–85 (in Japanese)
- Ohara N, He S, Parsekian AD, Jones BM, Rangel RC, Nichols IO, Hinkel KM (2022) Spatial snowdrift modelling for an open natural terrain using a physically-based linear particle distribution equation. *Hydrol Processes* 36:1. <https://doi.org/10.1002/hyp.14468>
- Okaze T, Niia H, Nishimura K (2018) Development of a large-eddy simulation coupled with Lagrangian snow transport model. *J Wind Eng Ind Aerod* 183:35–43. <https://doi.org/10.1016/j.jweia.2018.09.027>
- Okaze T, Niia H, Omiya S, Sunako S, Nishimura K (2019) Observation of snowdrift around two-dimensional fence during a drifting snow event. *JSSI & JSSE Joint Conference 2019 in Yamagata* 110 (in Japanese)
- Okaze T, Niia H, Omiya S, Sunako S, Kawashima R, Tanji S, Nishimura K (2022) Measurement of Snowdrift around a Fence with LiDAR for In-vehicle Use. *JSSI & JSSE Joint Conference 2022 in Sapporo* (in Japanese)
- Okaze T, Tominaga Y, Mochida A (2013) Development of new snowdrift model based on two transport equations of drifting snow density, numerical prediction of snowdrift around buildings using CFD (Part 2). *J Environ Eng ASCE* 139:149–156. [https://doi.org/10.1061/\(ASCE\)1090-0268\(2013\)139:1\(149\)](https://doi.org/10.1061/(ASCE)1090-0268(2013)139:1(149)) (in Japanese)
- Onodera N, Aoki T, Shimokawabe T, Kobayashi H (2013) A large-scale LES wind simulation using Lattice Boltzmann Method for a 10 km × 10 km area in Tokyo. *High Perf. Comput. Symp.* 123–131 (in Japanese)
- Palm SP, Kayetha V, Yang Y, Pauly R (2017) Blowing snow sublimation and transport over Antarctica from 11 years of CALIPSO observations. *Cryosphere* 11(6):2555–2569. <https://doi.org/10.5194/tc-11-2555-2017>
- Shiotani M (1953) Note on the vertical distribution of density of blowing snow in the snow storm. *Seppyo* 15:6–9 (in Japanese)
- Smagorinsky J (1963) General circulation experiments with the primitive equations. I. the basic experiment. *Mon Wea Rev* 91:99–164. [https://doi.org/10.1175/1520-0493\(1963\)091%3C0099:GCEWTP%3E2.3.CO;2](https://doi.org/10.1175/1520-0493(1963)091%3C0099:GCEWTP%3E2.3.CO;2)
- Suga K, Kuwata Y, Takashima K, Chikasue R (2015) A D3Q27 multiple-relaxation-time lattice Boltzmann method for turbulent flows. *Comp & Math App* 69:518–529. <https://doi.org/10.1016/j.camwa.2015.01.010>
- Sugiura K, Maeno N (2000) Wind-tunnel measurements of restitution coefficients and ejection number of snow particles in drifting snow: Determination of splash functions. *Bound-Layer Meteorol* 95:123–143
- Tabler RD (1994) Design guidelines for the control of blowing and drifting snow. *Strategic Highway Research Program Report SHRP-H-381*.
- Takeuchi M, Fukuzawa Y (1976) On the light attenuation and visibility in snow drift. *Seppyo* 38(4):165–170. https://doi.org/10.5331/seppyo.38.4_165 (in Japanese)
- Tanji S, Inatsu M, Okaze T (2021) Development of a snowdrift model with the lattice Boltzmann method. *Prog Earth Planet Sci* 8:57. <https://doi.org/10.1186/s40645-021-00449-0>
- Uematsu T, Nakata T, Takeuchi K, Arisawa Y, Kaneda Y (1991) Three-dimensional numerical simulation of snowdrift. *Cold Reg Sci Tech* 20:65–73. [https://doi.org/10.1016/0165-232X\(91\)90057-N](https://doi.org/10.1016/0165-232X(91)90057-N)
- Wang X, Shangquan YQ, Onodera N, Kobayashi H, Aoki T (2014) Direct numerical simulation and large eddy simulation on a turbulent wall-bounded flow using Lattice Boltzmann Method and multiple GPUs. *Math Problem Eng* 742432. doi:<https://doi.org/10.1155/2014/742432>.
- Wang Z, Jia S (2018) A simulation of a large-scale drifting snowstorm in the turbulent boundary layer. *Cryosphere* 12:3841–3851. <https://doi.org/10.5194/tc-12-3841-2018>
- Werner H, Wenglem H (1991) Large-eddy simulation of turbulent flow over and around a cube in a plate channel. In: *Proceedings of 8th symposium on turbulent shear flows* pp 155–158. https://doi.org/10.1007/978-3-642-77674-8_12.
- White F (1974) *Viscous fluid flow*. McGraw-Hill Inc, US, p 640
- Zwaafink CDG, Diebold M, Horender S, Overney J, Lieberherr G, Parlange MB, Lehning M (2014) Modelling small-scale drifting snow with a Lagrangian stochastic model based on large-eddy simulations. *Bound-Layer Meteorol* 153:117–139. <https://doi.org/10.1007/s10546-014-9934-2>
- Zwaafink CDG, Mott R, Lehning M (2013) Seasonal simulation of drifting snow sublimation in Alpine terrain. *Water Resour Res* 49:1581–1590. <https://doi.org/10.1002/wrcr.20137>

Publisher's Note

Springer Nature remains neutral with regard to jurisdictional claims in published maps and institutional affiliations.

Submit your manuscript to a SpringerOpen® journal and benefit from:

- Convenient online submission
- Rigorous peer review
- Open access: articles freely available online
- High visibility within the field
- Retaining the copyright to your article

Submit your next manuscript at ► [springeropen.com](https://www.springeropen.com)